UJMR, Conference Special Issue Vol. 9 No. 3. June, 2024, pp. 336 - 349

E-ISSN: 2814 – 1822; P-ISSN: 2616 – 0668

https://doi.org/10.47430/ujmr.2493.041

Received: 13th February, 2024 **Accepted:** 15th June, 2024

Electricity Generation by a Phototrophic Bacterium in a Glucose–Fed Double Chambered Microbial Fuel Cell Using a Fabricated 3D Anode Electrode

***[1]Aliyu, A. A., [2]Dahiru, R.**

[1]Department of Environmental Sciences, Gobarau College of Health Sciences and Technology Katsina, Katsina, Nigeria
[2]Department of Pharmaceutical Sciences,College of Health Sciences and Technology Katsina (COHESKAT), Katsina, Nigeria
*Correspondence author: abdulkadir.albaba@gmail.com, +234 816 854 5234

Abstract

Over the past years, despite intensified research on microbial fuel cells (MFC), low power densities were recorded, reducing the productivity and economic viability of the process. This necessitated testing various MFC configurations, fabricating various electrodes, and evaluating various substrate types and species of electrogenic microorganisms to improve MFC performance. Despite the dual advantage of phototrophic bacteria (PTB), metabolizing organic waste substances and generating electricity, less research was conducted on the bacterium. Although a significant amount of energy is generated using unsustainable (fossil-based) materials in electrode fabrication, this study focuses on using sustainable materials like carbon cloth and graphite to fabricate a 3D anode electrode to exploit the maximum energy generated by PTB. The PTB used in this study was identified through morphological characteristics and biochemical tests (catalase and oxidase) and confirmed using a molecular technique: 16S rRNA sequencing. Preliminary results indicated that the PTB was gram-negative, spherical in shape, non–motile, and facultatively anaerobic bacterium. Analysis of the 16S rRNA partial sequence was conducted in GenBank databases. 100 significant sequences with the lowest and highest similarities of 84.10% and 98.76% were recorded, respectively. Of these, 13 strains had the highest similarities of >90%, all belonging to the genus Dysgonomonas, with D. oryzarvi Dy73 (98.76%) as the closest. Reduced graphene oxide (rGO) used as the anode was prepared using Hummer's method by depositing the rGO on nickel (Ni) foam which changed the colour of Ni from grey to black after depositing and annealing. In addition to the SEM images, which showed a continuous multi–layered 3D scaffold on the Ni, the cyclic voltammetry (CV) analyses indicated an increase in the electrochemical activities of the rGO–Ni electrode compared to Ni. The CV also confirmed the bacterium to be electrochemically active. The 100 mL glucose–fed two–chamber MFC were separately run with the Ni and rGO-Ni as anode electrodes in a batch mode for 11 days, while carbon cloth was used as the cathode for both runs. An approximate 0.58 W/m^2 power density was recorded for Ni, but eight–fold of Ni's, 4.9 W/m^{2}was generated by rGO–Ni. The study demonstrated that using fabricated 3D rGO-Ni as anode electrode can increase the microbial adhesion and power density of bacterium in MFC, thereby providing a more applicable and sustainable alternative to bioelectricity generation.

Keywords: *phototrophic bacteria (PTB), microbial fuel cell (MFC), 3D electrode, Dysgonomonas*

INTRODUCTION

Energy is essential for life in the twenty-first century, considering its significance in various sectors, as evidenced by the constant rise in global energy consumption. Since their discovery, fossil fuels have been the major global energy provider (more than 80%) (Alimonti, 2018). The intensifying efforts to extract more fossil fuels and their extensive applications due to increasing demand resulted in more carbon dioxide production, raising global concerns (Guo *et al.*, 2022). According to the United Nations (UN), 75% of greenhouse gas (GHG) emissions result from fossil fuel use, consequently destabilizing the world's environmental equilibrium and causing the global threat of climate change accelerated by continuous deforestation (Sonawane *et al.*, 2017).

E-ISSN: 2814 – 1822; P-ISSN: 2616 – 0668

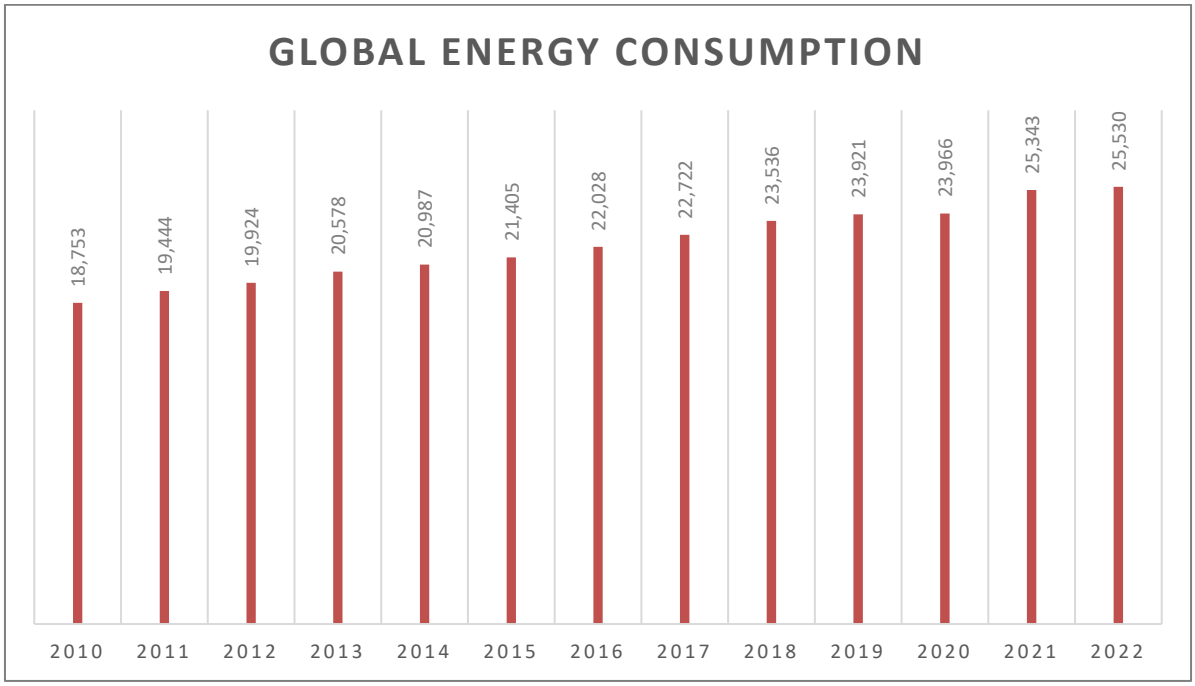

Figure 1. Global energy consumption between 2010 to 2022 (Source: Statistica, 2024)

A significant increase in global energy demand has been experienced for the past decades. With the progressive increase in global energy demands, as shown in Figure 1, and the Sustainable Development Goals (SDGs) call for sustainable, affordable, and clean energy, the race for improving and innovating various techniques intensifies exponentially. Several renewable, sustainable, and eco–friendly energy alternatives like solar, wind, and hydropower have been developed and improved. Although these renewable energy technologies (RE) are now key contributors to the modern energy mix globally with little or no emissions of GHGs, their cost of installation/operation is noticeably expensive, making it unaffordable and inaccessible to nearly 775 million people around the world (International Renewable Energy Agency, IRENA, 2024; International Energy Agency, IEA, 2022).

Bioenergy results from utilizing organic, agricultural, and industrial wastes to generate energy with no or minimal GHG emissions (Roder and Welfle, 2019). Ghangrekar *et al.* (2022) stated bioelectricity is the most focused area in bioenergy. Bioelectricity involves converting the stored chemical energy in organic substances into electrical energy by microorganisms (aerobically or anaerobically).

In 1911, Potter introduced the idea of the Microbial Fuel Cell (MFC), an electrochemical cell with electrodes (anode and cathode) and chamber(s) containing the microorganism(s) and electrolytes (organic waste) to be degraded for bioelectricity generation (Potter 1991; Haruna *et al.*, 2023). Potter's initiative used *E. coli* and *Saccharomyces* with platinum electrodes to generate energy. Unfortunately, due to the insignificant amount of energy generated, researchers showed no further interest until 1931, when Cohen used a similar method to generate a potential voltage of 35 V (Logan, 2005). Over time, interest in this research area catapulted, with an average publication record of 1,244 articles annually between 2010–2022, according to the Web of Science (2023) database.

In addition to generating bioelectricity, MFCs provide an avenue for wastewater treatment, thereby reducing the volume of global wastewater (380 billion m^3), which is expected to increase by 51% by 2050, according to the European Investment Bank (EIB, 2022). Moreover, 80% of global infectious diseases are caused by untreated wastewater, resulting in 13 million deaths annually (Wolf et al., 2023).

The performance of an MFC is majorly dictated by the MFC configuration, microbial electrochemical activity, substrate type, electrode type, and electrode material (Pant *et al.*, 2010; Kim *et al.*, 2011). Several configurations such as mediator/mediatorless MFC, photoMFC, upflow MFC, and stacked–MFC have been made to improve MFCs' performance, and that resulted in a significant increase in power density (PD) and current density (CD)

generation (Jang *et al.*, 2004; Aelteman *et al.*, 2006). In a recent study, Sato *et al.* (2023) incorporated an MFC with a hydroponic system (MFC–Hyp) to generate a maximum PD and CD of 523.9±50 mW/m^2 and 2,676.7±340.7 mA/m^2, respectively. Subsequently, another study used a photo–MFC configuration to generate a maximum PD of 280 mW/m^2 with photocathode and bioanode (Wang *et al.*, 2023).

Furthermore, other developments were recorded by Shirkoshi *et al.* (2022) with microfluidic–MFC, which produced a maximum open circuit voltage (OCV) of 1.295 V, PD of 21,111 W/m^3, and CD of 140,000 A/m^3. Apollon *et al.* (2023a) also recorded a PD and CD of 46.97 ± 0.67 mW/m^2 and 77.45 ± 0.24 mA/m^2 using plant–based MFC clay embedded with *Stevia rebandiana*. While with sediment-MFC configuration, a significant PD of 1,056.6 W/m^2 was obtained by Mejia-Lopez *et al.* (2023). However, most configurations are on the research level, while some have been applied on an industrial scale. In this study, double-chambered MFC was used because of its availability, ease to scale-up, and efficiency (Wang *et al.*, 2023).

Not only did electrode materials such as carbon, graphene, polyaniline, platinum, and stainless–steel fibre play a vital role in enhancing MFC performance, but also the type, i.e., three-dimensional (3D) and two-dimensional (2D) as well, since it influences microbial colonisation and hence the electrochemical activity of the microbe (Qi *et al.*, 2018). Several studies have indicated electrode materials' role in microbial adhesion and performance. Tan *et al.* (2018), using in-situ Co_3O_4 nanoparticles modified nitrogen–doped graphene (3D GN–Co_3O_4) cathode, recorded 578±10 mW/m^2 and 0.45±0.01 V as PD and OCV, respectively, which is fivefold higher compared to the 177.03 mW/m^2 generated using plain carbon cathode by Piskin and Genc (2023).

The differences in concentration and type of substrate also showed an improved energy generation in MFCs, as Tian et al. (2017) evaluated. Likewise, Guo *et al.* (2022) stated that an increase in electricity production through electron transfer efficiency was noticed when acetate was used as a co–substrate. Apollon *et al.* (2023b) reported that using livestock urine as substrate resulted in a maximum PD and CD of 110.72±0.42 mW/m^2 and 277±0.04 mW/m^2, respectively.

Qi *et al.* (2018) suggested that sustainable energy could be generated by tapping on the potential of phototrophic bacteria (PTB). They further recorded an OCV and short–circuit current (ISC) of 0.96 V and 0.75 A/m^{2}respectively, with a PTB. Several studies of pure or mixed culture of PTB and other electrogenic bacteria had been conducted: *Geobacter metallireducens* recorded a PD of 2.2 mW/m^2; *Rhodospirillum rubrum* 1.25 W/m^2; and *Rhodopseudomonas palustris* strain DX–1 2.7 W/m^2 (Xing *et al.*, 2008).

Other MFC applications include energizing low–power consuming devices like small telemetry systems, wireless sensors, biosensors (for monitoring biological oxygen demand), and health condition monitors (Kumar *et al.*, 2017). These developed devices include EcoBot I, EcoBot II, Slugbot, Gastrobot, and Chew Chew (Du *et al.*, 2007; David and Higson, 2007).

Several modifications to enhance the performance of MFCs has been conducted; however, despite MFCs' promising potential, the ideal low–power generation is a significant setback to its applicability (Wang *et al.*, 2013). PTB uses light energy to degrade waste substances while generating electricity, but there is a paucity of research on harnessing and analyzing the electrochemical potential of PTB (Fischer, 2018). This study will assess and improve the electrochemical potential of a PTB by fabricating a 3D anode electrode using glucose as the substrate in a two–chamber MFC.

MATERIALS AND METHODS

A pure culture of the PTB previously isolated in another study was sub–cultured on agar and broth of 112 medium. Streak–plating method was adopted for the inoculation on an agar medium. The medium composition (L^{-1}) was 1.0 g of K_2HPO_4, 0.5 g of $MgSO_4$, 10.0 g of yeast extract, and 20.0 g of agar (only for agar medium). The culturing was done at 28–35℃ and 7.0–7.2 of temperature and pH, respectively, under an anaerobic, aseptic, and light mode for optimal growth. The bacterial growth (optical density)was monitored using a spectrophotometer at a wavelength of 660 nm (OD_{660}) (Kodama *et al.*, 2012).

Morphological Study of the PTB

The gram staining technique and motility test were carried out according to the standard procedure to characterise the PTB in this research. According to Tripathi and Sapra

(2023), a single colony of the PTB was picked from a 24-hour agar plate using a sterile inoculating loop, smeared on a cleaned glass slide, and left to dry. The smear was first flooded with crystal violet stain for 60 secs, followed by gram's iodine for 60 secs, a few drops of ethanol at 45⁰, and then safranin for 60 secs. Distilled water was used to wash the slide at each step before applying another reagent. After adding a drop of immersion oil and coverslip, a compound microscope was used to observe the slides.

The hanging drop method was applied to examine the bacterial motility. A single colony from the agar plate was picked using a sterile inoculating loop and placed in distilled water on a cleaned circular depression glass slide. Paraffin wax was used to surround the circular depression on the glass slide. With the help of a coverslip, the glass slide was fixed in an upside–down orientation on the compound microscope, and the bacterium was examined (Kodama *et al.*, 2012).

Biochemical Tests

The two biochemical tests, catalase and oxidase, were conducted. One drop of PTB broth was set on a cleaned, labelled glass slide for the catalase test. While hydrogen peroxide (30% v/v) was the catalase reagent, a few drops were released on the bacteria and left for a few minutes to observe. Bubbles indicate a positive result, and their absence is negative (Azhary *et al.*, 2020).

The oxidase test was done with a commercial oxidase reagent, Becton (5 mL). One drop of the bacterial suspension was also placed on a cleaned labelled glass slide. The reagent was deposited according to the manufacturer's instructions on the bacterial drop and allowed for a few minutes before analysing. The result is positive when the color changes to dark purple within 10 secs, delayed positive when it takes 60-90 secs, and negative when it does not change longer than 120 secs (Dharmappa *et al.*, 2022).

Polymerase Chain Reaction (PCR)

Colony PCR further studied the bacterium to amplify the 16S rRNA sequence. A single colony from an agar plate containing pure cultures of the PTB isolate was picked and suspended in 15 uL of distilled water, boiled in a PCR thermocycler for 10 mins, and centrifuged at 20,000 rpm for 5 mins. 1 uL of the supernatant was used as the DNA template.

The universal primers 27F (5′–AGAGTTTGATCMTGGCTCAG–3′) and 1492R (5′–GGTTAC CTTTGTTACGACTT–3′) were used in this study. The PCR mixture contained 50 uL per reaction: 25 uL of GoTaq green, 1 uL of each of 27F and 1492R primers, 1 uL of DNA template, and 22 uL of ultrapure water. The PCR amplification was done in the GeneAmp PCR System 9700 thermocycler (Perkin Elmer, GA9700) with an optimised amplification program of 1 cycle at 95℃ for 2 mins, followed by 40 cycles of denaturation at 95℃ for 45 secs, annealing at 55℃ for 45 secs, extension at 72℃ for 30 secs, and a final extension of 1 cycle at 72℃ for 5 mins (Sharma *et al.*, 2016).

Gel electrophoresis of the PCR product was performed using 1% gel prepared by weighing 1.5 g of agarose powder and mixing it with 250 mL of Tris–acetate buffer (TAE buffer). The solution was microwaved for 2–3 mins, cooled to room temperature, and 5 uL of ethidium bromide was added before pouring it into the comb tray to solidify. After solidification, 1,500 bp was deposited as the loading band in the first well. The electrophoresis machine was set for 30 mins at 80–120 V, and the products were visualised in the darkroom using ultraviolet (UV) light (Lee *et al.*, 2012).

The PCR product was sequenced via the Sanger sequencing technique with initial ribonuclease treatment followed by DNA purification. The 16S rRNA gene sequence was obtained through Amplicon sequencing using NGS–7000 series. The obtained sequence was extracted using Sequence Scanner (SeqScan v2). The GenBank database blasted the extracted sequence using Nucleotide BLAST (blastN). Using the neighbour–joining tree method, a phylogenetic tree was constructed based on 100 related 16S rRNA gene sequences using molecular evolutionary genetics analysis (MEGA 11) (Tamura *et al.*, 2021).

Preparation of Electrode

Graphene Oxide (GO) Preparation

The Hummer method was used to prepare the GO from graphite powder, as adopted by Wang *et al.* (2013). The graphite powder weighing 50 mg was mixed with 23 mL and 10 mL of concentrated H_2SO_4 and concentrated HNO_3, respectively, in a cooled ice bath container, followed by a slow addition of 3 g $KMnO_4$. The

solution was heated for 3 h at 35℃ and then diluted with 40 mL of deionised water, followed by 200 mL of deionised water 12 h later, and subsequently, 3 mL of 30% v/v/ H_2O_2 was slowly added. The solution was centrifuged at 1,500 rpm for 30 mins, and the residue of graphite oxide was isolated and washed with deionized water before being resuspended in deionized water (500 mL). The aqueous solution was sonicated for 2 h to form layered GO sheets.

Reduced Graphene Oxide (rGO) Sheets Deposition on Nickel Foam (Ni)

Initially, nickel (Ni) foam was washed with diluted concentrated H_2SO_4 and placed in an oven at 60℃ for 12 h. The Ni was then transferred into a 100 mL Teflon liner (hydrothermal reactor) filled with 50 mL of the sonicated aqueous GO solution, and the reactor was settled in an oven at 120℃ for 5 h. After 5 h, it was allowed to cool down to room temperature, washed with deionized water, and air-dried. To increase the electrical conductivity and firmness of the rGO-Ni, annealing was performed at 400℃ for 30 mins. The concentration of rGO in the solution was measured at 1 mg/mL (Wang *et al.*, 2013).

Field Emission Scanning Electron Microscopy (FESEM)

The FESEM of Ni and rGO-Ni was conducted at the Department of Physics, Universiti Malaya, using the Joel (JSM-7600F) microscopy model. The secondary electron image (SEI)resolution and X-ray beam diameter were adjusted at 5 kV and 10 mm using the EDX-Oxford instrument. Images were obtained at different magnifications and diameters (Lawan *et al.*, 2018).

Cyclic Voltammetry (CV)

The CVs were performed in a three-electrode set-up using an electrochemical workstation potentiostat: Eco Chemie (Autolab PGSTAT302). Ni and rGO-Ni were used as the working electrodes (WEs), Ag/AgCl as the reference electrode (RE), and the platinum wire as the counter electrode (CE). The WEs were cleaned with ethanol and washed with deionised water before use.

The scan rate was set at 50 mV/s, and the potential ranges at 0-1 V. Measurements were taken repeatedly in 100 mM phosphate buffer solution (PBS) of 7.0 pH at room temperature and atmospheric pressure under aerobic and anaerobic conditions with and without substrate (glucose). Voltammograms were obtained via the computer software General Purpose Electrochemical System (GPES) v4.9 (Sharma *et al.*, 2016).

Constructing the Microbial Fuel Cell (MFC)

A 100 mL two-chamber (50 mL each chamber) glassware MFC was used, as shown in Figure 2. Nafion NR-212 membrane was employed as the proton exchange membrane (PEM). The Nafion was pre-treated, as Rahmani et al. (2020) and Cheng et al. (2016) described. Originally, the membrane was boiled four times in distilled water, 30% v/v H_2O_2, 0.5M H_2SO_4, and finally, distilled water again at 80℃ for 1 h each. The membrane was washed consecutively after every boiling before being put aside in distilled water for further use.

The electrodes, anodes (Ni/rGO-Ni), and cathode (carbon cloth) were 1×2 cm each. The anodes were subjected to pre-treatment to enhance electron transfer and microbial adhesion, as Cheng et al. (2016) mentioned. The electrodes were immersed in two chemicals: 30% v/v isopropanol overnight and 30% v/v H_2O_2 for 24 hours. The electrodes were washed with distilled water and dried thoroughly at 100℃ at first and between the chemicals' immersion. Contrary to the anode, as Rahmani et al. (2020) stated, the cathode was pre-treated by soaking in acetone for 20 mins and later boiling in 0.1 M of HCl for 15 mins.

The glucose-fed MFC was sterilised with ethanol first. Glucose (100 mM) was the substrate used. The anolyte consisted of the substrate, bacterial stock at OD_{660} nm = 2, and 100 mM of PBS at 7.0 pH, while the catholyte was composed of 100 mM potassium ferricyanide. Although nitrogen gas was used to flush out oxygen in the anode chamber, so an anaerobic condition is maintained, the cathode chamber was left aerobic, as demonstrated in Figure 2. The MFC was connected to an external load of 1 kΩ for all experiments, the electrochemical station, and measurements were taken from GPES (v4.9) software. Experiments were run in batch mode, and each experiment was conducted twice to enhance data accuracy. The power was calculated using P=I*V, and the power densities were calculated based on the anode area (2 cm^2 or 0.0002 m^2) (Haruna *et al.*, 2023).

E-ISSN: 2814 – 1822; P-ISSN: 2616 – 0668

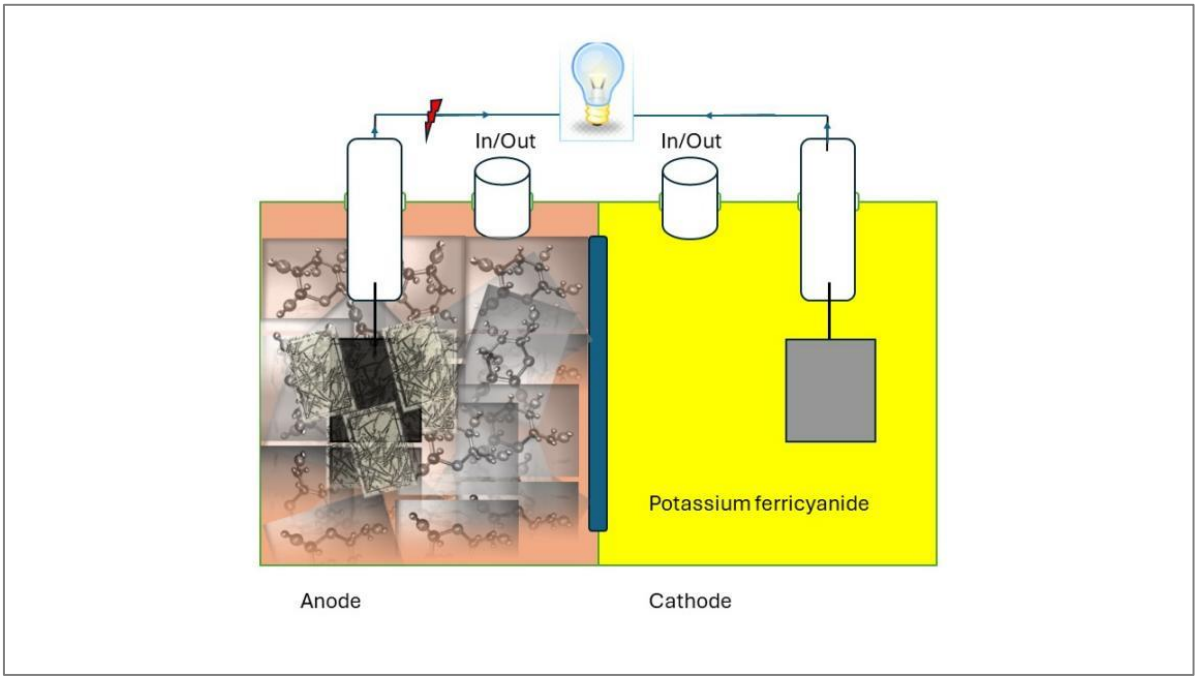

Figure2. Two–chambered MFC configuration used within the Study
(Nafion was used as the PEM, rGO–Ni as the anode, and carbon cloth as the cathode while the anode chamber remained anaerobic and the cathode chamber air–exposed).

RESULTS

Morphological Study

The bacterial colonies on the agar 24 h later formed a smooth, circular, milky color, less than 1 mm in diameter. On the contrary, the bacterial broth showed a dense reddish color at day 10, while the OD measured at 660 nm was 2.

The observed microscopy of the gram staining reaction showed it to be a chain–like red bacterium with an approximate size of 1.2×1.4 um. The motility examination of the bacterium revealed no movement on the slide completely. In addition, there was no flagellum or sporulating seen.

Biochemical Tests

Consequently, both the slides of catalase and oxidase tests, when observed, produced no reaction after 2 mins. The absence of air bubbles on the catalase slide showed the bacterium does not produce catalase enzyme hence it is catalase–negative.

The inability of the oxidase slides to change pointed out that the bacterium to be oxidase–negative. This further indicated that the bacterium does not undergo aerobic respiration, confirming it to be anaerobic. It was also observed that the presence of oxygen affects the growth rate of the bacterium, ultimately influencing the performance of the MFC.

Polymerase Chain Reaction (PCR)

The gel electrophoresis results showed an estimated 1,200 bp band of the PCR product under UV light. A partial 16S rRNA sequence of 1,211 bp was acquired from the extracted sequence. The blast N analysis of the 16S rRNA partial sequence in the GenBank database revealed 100 significant strains of microorganisms with similarities ranging from 84.10% to 98.76%.

Of the 100 strains of 16S rRNA partial sequences deposited in GenBank, 13 have the highest similarities (>90%), all from the genus *Dysgonomonas*. Table 1 shows that *Dysgonomonas oryzarvi* Dy73 has the closest (98.76%) sequence similarity, and *Dysgonomonas capnocytophagoides* CDC F9047 (90.36%) has the farthest similarity. This analysis suggested that the bacterium belongs to the genus *Dysgonomonas*.

E-ISSN: 2814 – 1822; P-ISSN: 2616 – 0668

Table 1: The 13 strains with the highest similarities (>90%) to the PTB

S/No.	Strains	Homology (%)
1.	***Dysgonomonas oryzarvi* Dy73**	**98.76**
2.	*Dysgonomonas mossii* DSM 22836 JCM 16699	98.60
3.	*Dysgonomonas mossii* CCUG 43457	98.51
4.	*Dysgonomonas termitidis* JCM 30204	93.96
5.	*Dysgonomonas gadei* ATCC BAA-286 JCM 16698	93.64
6.	*Dysgonomonas gadei* ATCC BAA-286 1145589	93.39
7.	*Dysgonomonas massiliensis* Marseille-P4356	93.17
8.	*Dysgonomonas hofsadii* JCM 17038	92.08
9.	*Dysgonomonas hofsadii* MX 1040	92.00
10.	*Dysgonomonas alginatilytica* HUA-2	91.23
11.	*Dysgonomonas capnocytophagoides* JCM 16697	91.10
12.	*Dysgonomonas macrotermitis* Dys-CH1	90.90
13.	*Dysgonomonas capnocytophagoides* CDC F9047	90.36

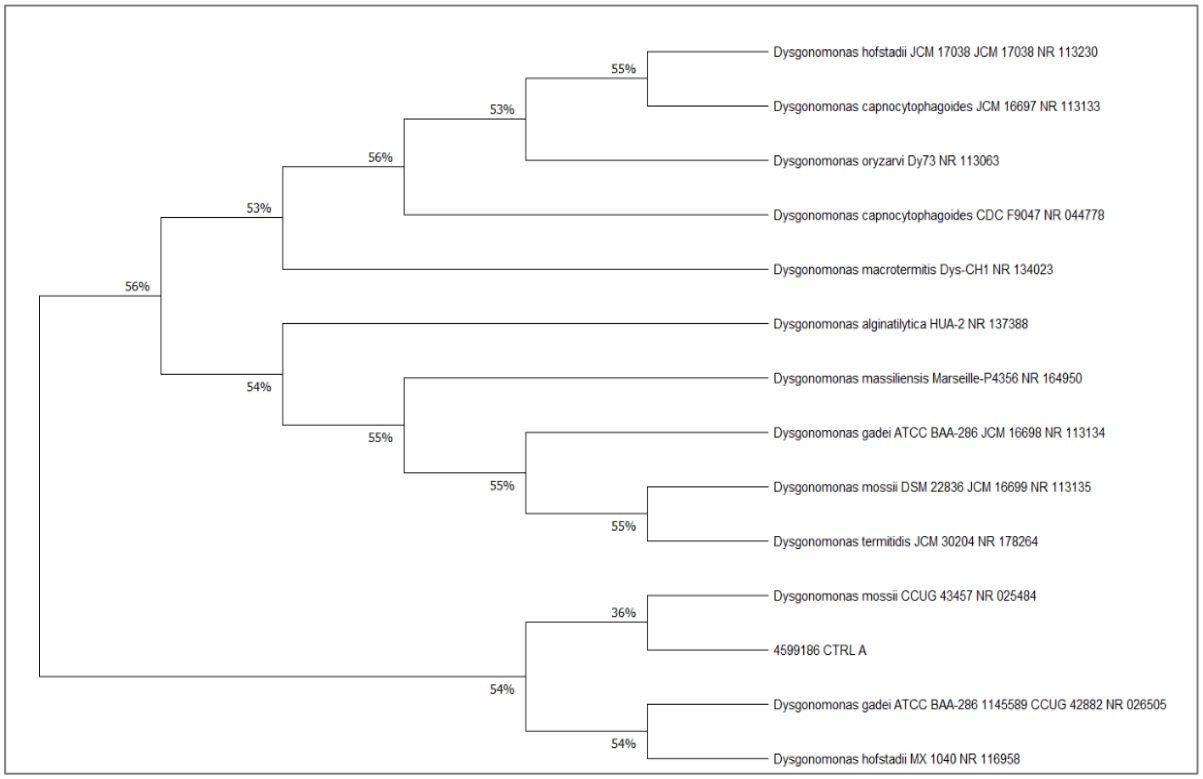

Figure3. Phylogenetic tree with the PTB's inquiry ID as 4599196 CTRL A.

The bacterium's phylogenetic tree (Figure 3) was created in the molecular evolutionary genetics analysis (MEGA 11) using the neighbour-joining method as mentioned in the methods. The PTB has not been reported in MFCs before, and this could be due to the absence of cytochrome enzyme, which is responsible for electron transfer during bacterial metabolism (Robb, 2020).

Electrode Preparation

The change in Ni color to black after rGO deposition indicated the effectiveness of the process (Figure 4a and b). Despite the annealing at 400°C for 5 h, the flexibility remained intact with no fragmentation when bent (Figure 4c). This makes the electrode apt for any MFC type and scaling-up application.

As revealed by the SEM images, the Ni was completely embedded with the rGO (Figure 5e and f), while Figure 5d confirmed multi-layered GO sheets in a continuous 3D scaffold with pores. These pores accommodate more bacterial adhesion, which increases electrochemical

activities, thereby enhancing the overall performance of the MFC.

As shown in Figure 4b, the change in the colour of Ni demonstrated rGO deposition. Further examination through SEM images proved the complete embedment of rGO onto Ni to form the 3D rGO–Ni electrode.

The CV analyses under the anaerobic and aerobic conditions with or without glucose showed oxidation and reduction peaks against the saturated RE: Ag/AgCl. The aerobic CVs with and without substrate revealed uncleared curves for Ni and rGO–Ni. In addition, the least maximum redox peaks were obtained in the aerobic treatment without substrate:0.07 nA(Ni) and 33.6 nA (rGO–Ni) (Figure 6a and e). Cleared curves for anaerobic with and without substrate were seen. .

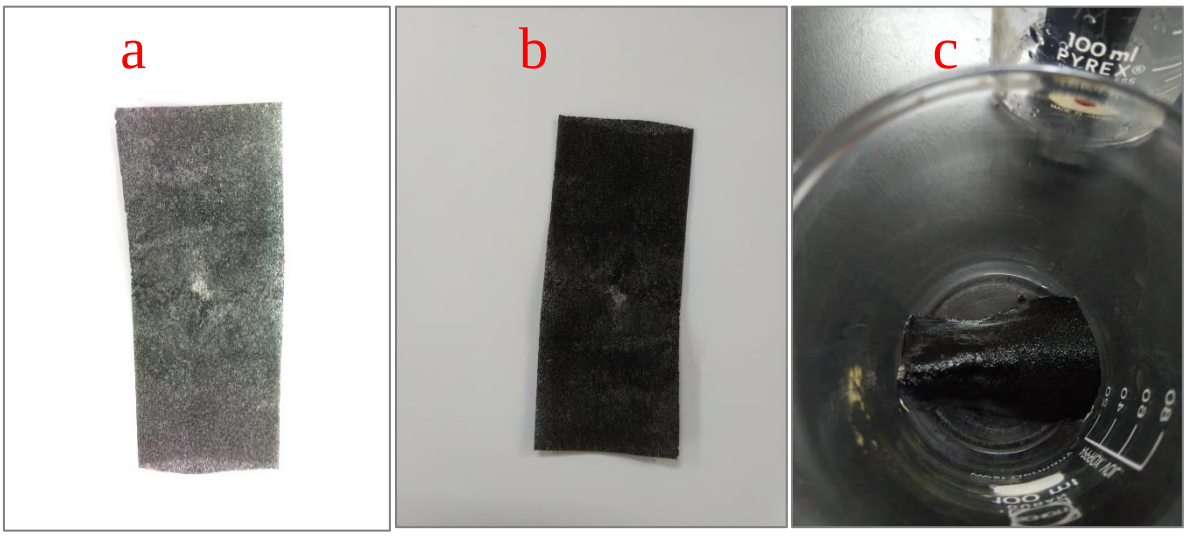

Figure4. (a) Ni before rGO deposition, (b) Ni after deposition and annealing of rGO to form the 3D rGO–Ni electrode, and (c) bending of the rGO–Ni, which confirmed the intactness of its flexibility without fragmentation.

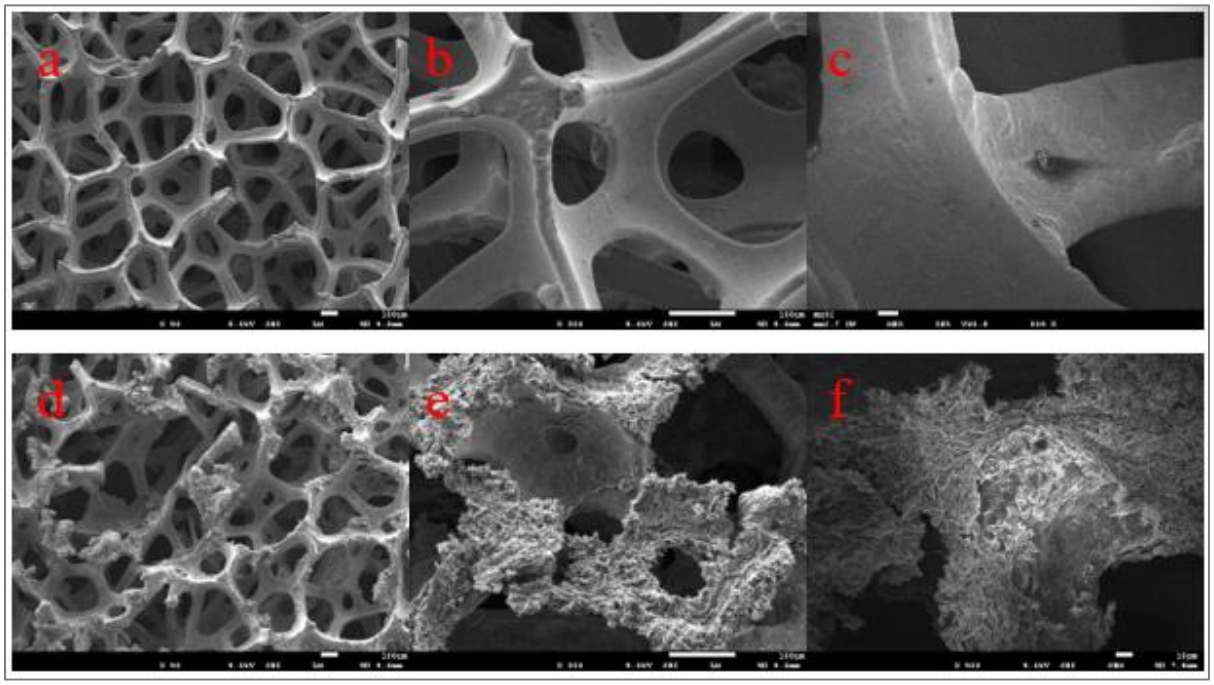

Figure5. SEM images of the Ni before deposition and annealing (a-c) and after deposition and annealing (d-f).

E-ISSN: 2814 – 1822; P-ISSN: 2616 – 0668

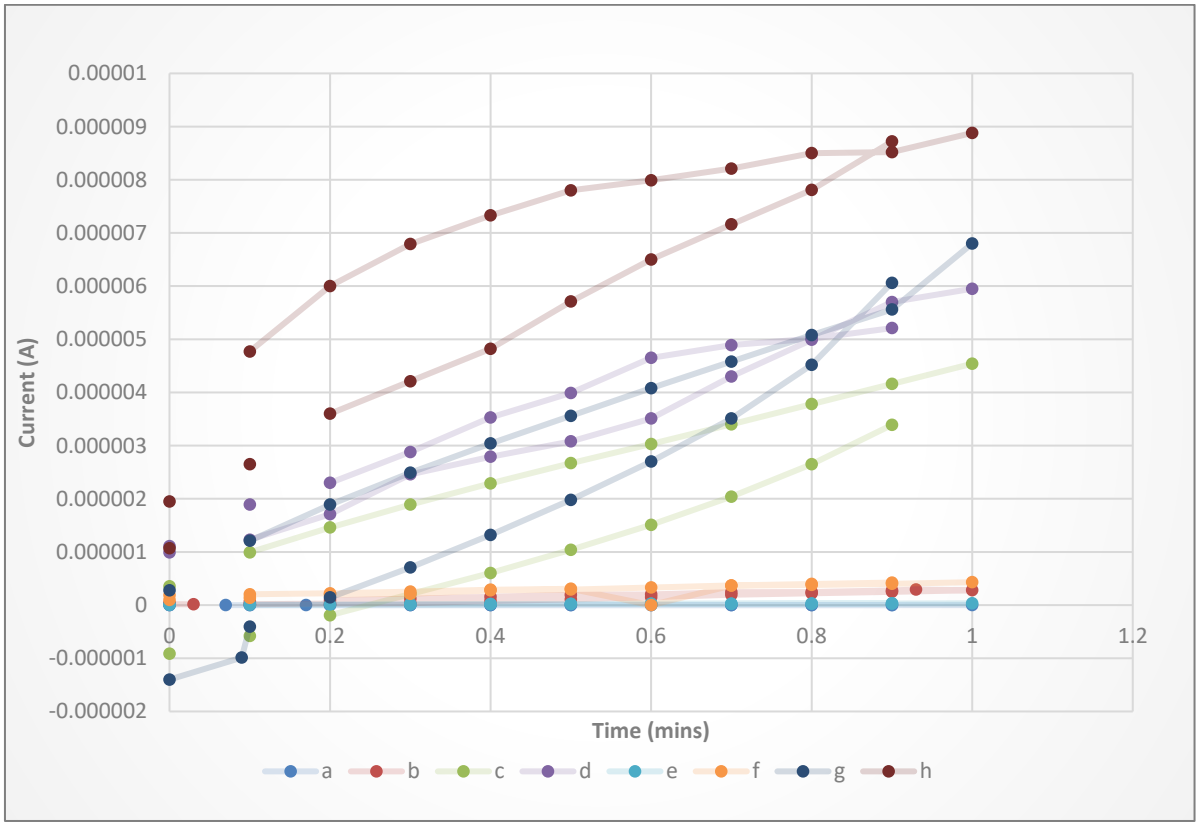

Figure6. CV measurements of Ni (a-d) and rGO–Ni (e-f) were measured. Both measurements of electrodes were taken under aerobic conditions without substrate (a and e), aerobic with substrate (b and f), anaerobic without substrate (c and g), and anaerobic with substrate (d and h).

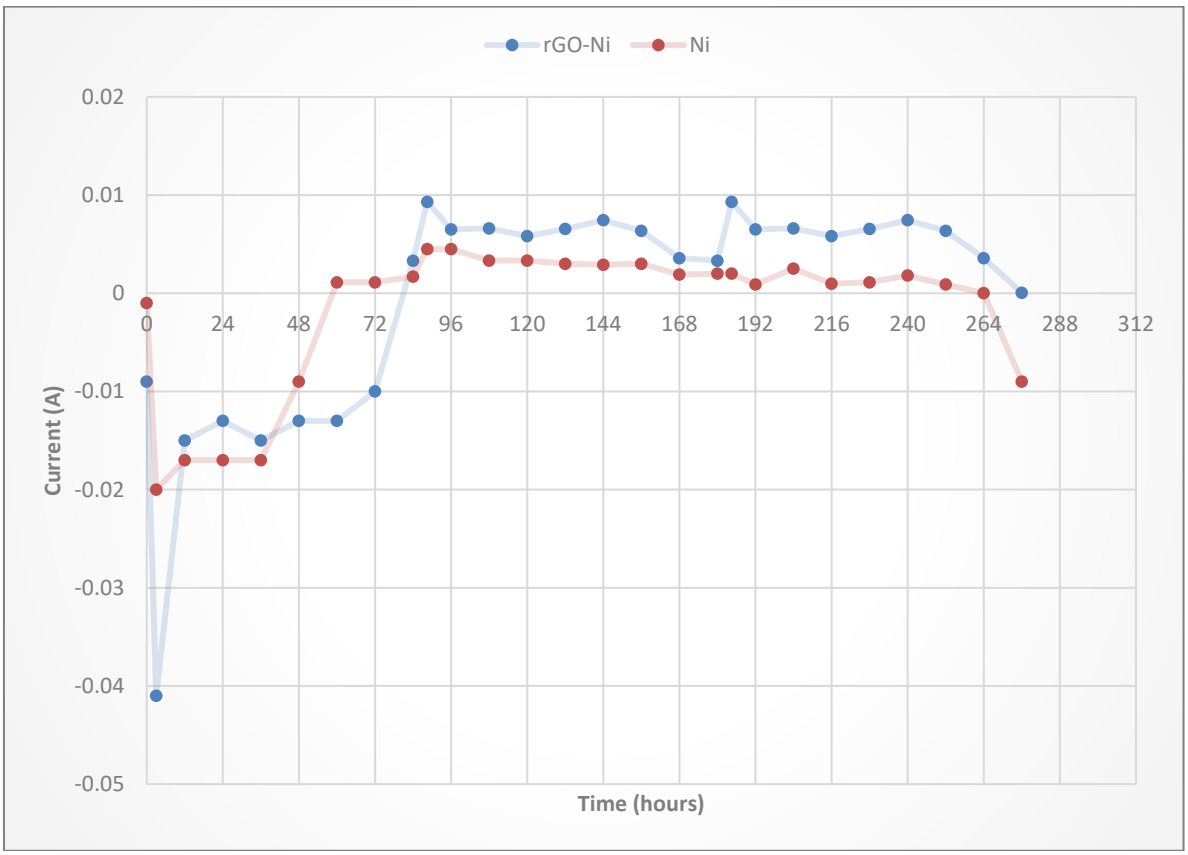

Figure7. The short–circuit current generated over 11 days in a batch mode MFC.

A maximum OCV of 0.99 V was measured from rGO–Ni while Ni recorded 0.34 V (Figure 8). Although this is four times lower than that obtained from the microfluid–MFC configuration by Shirkosh *et al.* (2022); however, it is also 100-fold higher compared to the 0.037 mV reported by Tou *et al.* (2019). This could result from the potential of the electrogenic bacterium and the enhanced 3D anode. Similarly, the rGO–Ni and Ni electrodes also exhibited a maximum ISC of 0.99 mA and 0.25 mA, respectively (Figure 8)

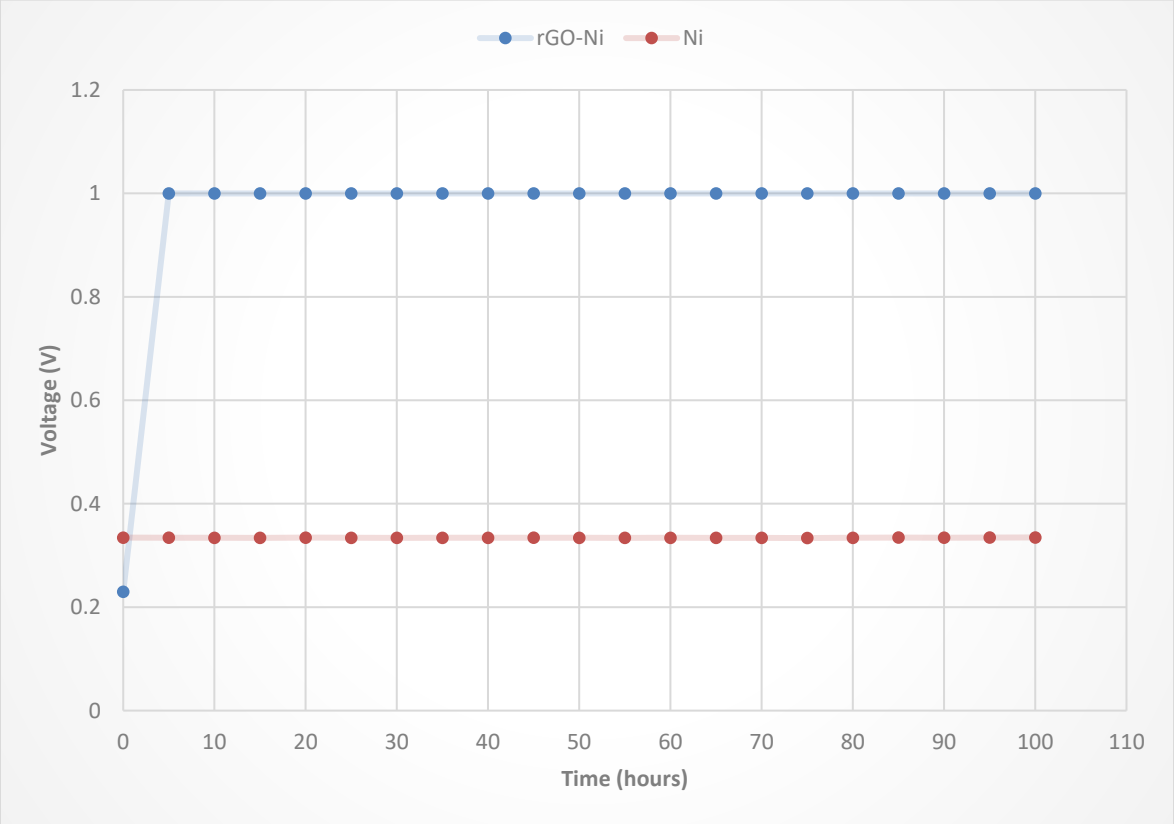

Figure8. The open circuit voltage is measured in a batch mode MFC.

DISCUSSION

The absence of retaining stain made it gram–negative, as discussed by several researchers. Neither a flagellum nor sporulation was seen. It has a chain–like coccus with circular colonies of less than 1 mm. This aligned with the characteristics of a non–motile, gram–negative bacterium, as Moyes et al. (2009) indicated.

The catalase result showed the bacterium to be anaerobic. Further observations revealed the presence of oxygen to affect the bacterial growth slightly. In the case of oxidase result, the bacterium cannot produce cytochrome oxidase enzyme, which enhances the electrochemical activity of electrogenic bacteria (Sharma *et al.*, 2016). This also indicates the presence or absence of the enzyme influences the power generation as stated by Sonaware *et al.* (2017). The molecular technique attested that the bacterium was likely *Dysgonomonas oryzarvi* Dy73, with 98.76% similarities as the morphological features, biochemical tests, and molecular study indicated (Kodama *et al.*, 2012).

The CVs conducted on Ni (Figure 6a-d) and rGO–Ni (Figure 6e-f) confirmed an enhanced electrochemical potential of the rGO–Ni electrode compared to the Ni. Not only did the CVs show that the bacterium is electrochemically active, but they also proved the effect of aerobic conditions on the electrochemical activity of the bacterium. Although small redox peaks were recorded in aerobic conditions without any substrate (Figure 6a and e), no changes were seen for the CV curves of both electrodes in anaerobic conditions with substrate (Figure 6d and h) except that the curves were clearer and attained the maximum peak in Figure 5h. As seen in Figure 5, the maximum peaks shared a similar pattern and were recorded from anaerobic treatments with a substrate, rGO–Ni (8.88 mA), followed by anaerobic with no substrate, rGO–Ni

(6.80 mA), anaerobic with a substrate, specifically Ni (5.95 mA), and anaerobic without substrate, also in the Ni treatment (4.54 mA). In summary, the fabricated 3D electrode accommodates more bacterial adhesion, as Wang *et al.* (2013) suggested, thereby increasing the power density produced by the MFC. Additionally, the material used, Ni foam, plays a significant role in being unharmed material and enhancing the bacterium's electrochemical productivity.

The maximum PD values of approximately 4.9 W/m^2 and 0.58 W/m^2 were calculated for rGO–Ni and Ni electrodes. This is significantly higher than studies conducted by Eslami *et al.* (2023) and Tou *et al.* (2019) that generated a PD of 0.7 mW/m^2 when graphite rod was used with *Saccharomyces cerevisiae* and 744 uW/m^2 using *Cholophytum comosum*, respectively. However, compared to the 3D GN–Co_3O_4 used by Tan *et al.* (2018), a notable maximum PD of 578±10 mW/m2 was recorded. This resulted from the modification and electrode material used, as Chen et al. (2014) and Hou et al. (2014) pointed out.

Approximately one-and-a-half folds of OCV, four folds of ISC, and six folds of PD were obtained from rGO–Ni compared to the Ni electrode, proving the effectiveness and efficiency of the continuous 3D scaffold electrode in increasing microbial colonisation as well as enhancing the electrochemical performance of the overall MFC. Furthermore, the cell ran for 11 days before the current started to decline progressively, suggesting the depletion of nutrients and possibly the removal of the organic matter in the anolyte. It was also deciphered that the cell could run for more than two weeks while electrochemically functioning.

CONCLUSION

The phototrophic bacterium in this study was a gram–negative, non–motile coccus in chains that is a facultatively anaerobic bacterium that belongs to the genus *Dysgonomonas*. Based on the CV, OCV, ISC, and PD values of the two electrodes, Ni (0.58 W/m^2) and rGO–Ni (4.9 W/m^2), this study established that the fabrication of a 3D rGO–Ni electrode increases microbial adhesion, colonisation, as well as the overall power density generated by the *D. oryzarvi* Dy73in the MFC providing more applicable, economically – viable, and sustainable alternative to bioelectricity generation. More importantly, this study demonstrated that 3D electrodes can further amplify MFC performance and could be scaled industrially. Further analyses to understand this bacterium's exact mechanism of exocellular electron transfer are recommended for future study.

ACKNOWLEDGEMENT

This research was supported by the Petroleum Trust Development Fund (PTDF), Nigeria.

REFERENCE

Aelterman, P., Rabaey, K., Pham, T. H., Boon, N., &Verstraete, W. (2006). Continuous electricity generation at high voltages and currents using stacked microbial fuel cells. *Environmental Science Technology*, 40, 3388–3394. **[Crossref]**

Alimonti, G. (2018). Our energy future starts from actual energy limits, *EPJ Web of Conferences*, *189*, 00003. **[Crossref]**

Apollon, W., Luna-Maldonado, A. I., Kamaraj, S.-K., Vidales-Contreras, J. A., Rodríguez-Fuentes, H., Gómez-Leyva, J. F., Maldonado-Ruelas, V. A., & Ortiz-Medina, R. A. (2023a). Self-sustainable nutrient recovery associated to power generation from livestock's urine using plant-based bio-batteries. *Fuel*, *332*, 126252. **[Crossref]**

Apollon, W., Kamaraj, S., Rodríguez-Fuentes, H., Florencio, J. G., Antonio, J. V., Verónica, M. M. & Isabel, A. L. (2023b). Bio-electricity production in a single-chamber microbial fuel cell using urine as a substrate, *Biofuels*, **[Crossref]**

Azhary, S.-M., Almofti, Y.-A., Mustafa, E. A., Fagirii, S.-A. (2020). Antibiotic resistance profile of bacterial isolates from dairy farms manure in Bahri locality, Sudan. International Journal of Modern Pharmaceutical Research, 4(5), 99-110.

Canfield, J., Goldner, B., Lutwack, R. (1963). NASA Technical report. Magna Corporation, Anaheim, CA;63

Chen, J. Y., Li, N., & Zhao, L. (2014). Three–dimensional electrode microbial fuel cell for hydrogen peroxide synthesis coupled to wastewater treatment. *Journal of Power Sources*, *254*, 316–322. **[Crossref]**

Cheng, P., Shan, R., Yuan, H. R., Shen, W. J., & Chen, Y. (2020). Bioelectricity generation from the salinomycin–simulated livestock sewage

in a Rhodococcus pyridinivorans inoculated microbial fuel cell. *Process Safety and Environmental Protection*, *138*, 76–79. **[Crossref]**

Cozzi, L., Wetzel, D., Tonolo, G. (2022). The pandemic, inflation and the energy crisis have set back global progress on universal access to electricity, which must be a top priority at COP27. International Energy Agency iea.org (accessed 03/03/2023).

Davis, F., Higson, S. P. J. (2007). Biofuel cells–Recent advances and applications. *Biosens Bioelectron*; 22,1224–35. **[Crossref]**

Dharmappa, D. C., Anokhe, A., & Kalia, V. (2022). Oxidase Test: A Biochemical Methods in Bacterial Identification. AgriCose-Newsletter, 3(1).

Du, Z., Li, H., Gu, T. (2007). A state–of–the–art review on microbial fuel cells: a promising technology for wastewater treatment and bioenergy. *Biotechnology Advance*; *25*, 464–82. **[Crossref]**

Eslami, S., Bahrami, M., Zandi, M., Fakhar, J., Gavagsaz-Ghoachani, R., Noorollahi, Y., Phattanasak, M., Nahid-Mobarakeh, B. (2023). Performance investigation and comparison of polypropylene to Nafion117 as the membrane of a dual-chamber microbial fuel cell. *Cleaner Materials,Vol. 8*, 100184. **[Crossref]**.

European Investment Bank, 2022. eib.org (accessed 03/03/2023).

Fischer, F. (2018). Photoelectrode, photovoltaic and photosynthetic microbial fuel cells. *Renewable and Sustainable Energy Reviews*, *Vol. 90*, 16-27. **[Crossref]**

Ghangrekar, M. M., & Nath, D. (2022). Microbial electrochemical technologies for wastewater treatment: insight into theory and reality. In *Clean Energy and Resource Recovery* (pp. 179–200). Elsevier. **[Crossref]**

Guo, H., Xie, S., Huang, C., Tang, S., Geng, X., & Jia, X. (2022). An electricity–generating bacterium separated from oil sludge microbial fuel cells and its environmental adaptability. *Environmental Science and Pollution Research*, 1–10. **[Crossref]**

Guo, K., Hassett, D. J., Gu, T. (2012). Microbial fuel cells: electricity generation from organic wastes by microbes. In: Arora R, editor. *Microbial biotechnology: energy and environment*. United Kingdom: CAB International; p. 162–89. **[Crossref]**

Haruna, S., Yusuf, H., Gumel, A. M., Buhari, A. S., & Abubakar, U. U. (2024). Generation of bioelectricity in microbial fuel cell using kitchen waste obtained from Dutse urban, Nigeria. Dutse Journal of Pure and Applied Sciences, 9(4a), 94-104. **[Crossref]**

Hou, J., Liu, Z., Yang, S., & Zhou, Y. (2014). Three-dimensional macroporous anodes based on stainless steel fiber felt for high-performance microbial fuel cells. Journal of Power Sources, 258, 204-209. https://doi.org/10.1016/j.jpowsour.2014.02.035.

Hu, H., Fan, Y., Liu, H. (2008). *Water Res.*, *42*, 4172–4178. **[Crossref]**

International Energy Agency, 2022. iea.org (accessed 03/03/2023).

International Renewable Energy Agency, 2024. irena.org (accessed 01/07/2024)

Jang, J. K., Pham, T. H., Chang, I. S., Kang, K. H., Moon, H., Cho, K. S., Kim, B. H. (2004). Construction and operation of a novel mediator– and membrane–less microbial fuel cell. *Process Biochemistry* 39(8),1007–1012. **[Crossref]**

Kim, H-W., Nam, J-Y., & Shin, H-S. (2011). Ammonia inhibition and microbial adaptation in continuous single-chamber microbial fuel cells. Lancet. 196. 6210-6213. **[Crossref]**.

Kodama, Y. & Watanabe, K. (2008). An electricity–generating prosthecate bacterium strain Mfc52 isolated from a microbial fuel cell. *FEMS Microbiology Letter288*, 55–61. **[Crossref]**

Kumar, R., Singh, L., Zularisam, A.W. (2017). Microbial Fuel Cells: Types and Applications. In: Singh, L., Kalia, V. (eds) Waste Biomass Management – A Holistic Approach. Springer, Cham. **[Crossref]**

Lawan, S. M., Abba, I., Bala, B. D., Abdullahi, A. Y., & Aminu, A. (2018). Clean energy generation using groundnut oil mill effluent with microbial fuel-cell. Nigerian Journal of Technology, 37(4), 1076. **[Crossref]**

Lee, P. Y., Costumbrado, J., Hsu, C. Y., & Kim, Y. H. (2012). Agarose gel electrophoresis for the separation of DNA fragments. Journal of visualized experiments: JoVE, (62), 3923. **[Crossref]**

Liang, H., Han, J., Yang, X., Qiao, Z., Yin, T. (2022). Performance improvement of microbial fuel cells through assembling anodes modified with nanoscale

materials. *Nanomaterials and Nanotechnology*, 12. [Crossref]

Logan, B. E., Regan, J. M. (2006). Electricity–producing bacterial communities in microbial fuel cells. *Trends Microbiology*; *14*, 512–8. [Crossref]

Mejía-López, M., Lastres, O., Alemán-Ramirez, J. L., Lobato-Peralta, D. R., Verde, A., Monjardín, J. J. G., López de Paz, P., Verea, L. (2023). Conductive carbon-polymer composite for bioelectrodes and electricity generation in a sedimentary microbial fuel cell. *Biochemical Engineering Journal*, *Vol. 193*, 108856. [Crossref]

Moyes, R. B., Reynolds, J., & Breakwell, D. P. (2009). Differential staining of bacteria: gram stain. Current Protocols in Microbiology, 15(1), A-3C. [Crossref]

Pant, D., Van Bogaert, G., Diels, L., Vanbroekhoven, K. (2010). A review of the substrates used in microbial fuel cells (MFCs) for sustainable energy production. *Bioresource Technology;101*, 1533–43. [Crossref]

Pişkin, E. D. & Genç, N. (2023). Multi response optimization of waste activated sludge oxidation and azo dye reduction in microbial fuel cell, *Environmental Technology*, [Crossref]

Potter, M. C. (1911). Electrical Effects Accompanying the Decomposition of Organic Compounds. *Proc R Soc Lond [Biol]*; *84*, 260–76. [Crossref]

Qi, X., Ren, Y., Liang, P., & Wang, X. (2018). New insights in photosynthetic microbial fuel cell using anoxygenic phototrophic bacteria. *Bioresource technology*, *258*, 310–317. [Crossref]

Rahmani, A. R., Navidjouy, N., Rahimnejad, M., Alizadeh, S., Samarghandi, M. R., & Nematollahi, D. (2022). Effect of different concentrations of substrate in microbial fuel cells toward bioenergy recovery and simultaneous wastewater treatment. *Environmental Technology*, *43*(1), 1–9. [Crossref]

Ren, H., Pyo, S., Lee, J. I., Park, T. J., Gittleson, F. S., Leung, F. C., ... & Chae, J. (2015). A highpower density miniaturized microbial fuel cell having carbon nanotube anodes. *Journal of Power Sources*, *273*, 823–830. [Crossref]

Robb, A. J., Knorr, E. S., Watson, N., & Hanson, K. (2020). Metal ion linked multilayers on mesoporous substrates: Energy/electron transfer, photon upconversion, and more. Journal of Photochemistry and Photobiology A: Chemistry, 390, 112291. [Crossref]

Röder, M., Welfle, A. (2019). Bioenergy, Editor(s): Trevor M. Letcher, Managing Global Warming, Academic Press, 12, 379-398. [Crossref]

Sato, C., Apollon, W., Luna-Maldonado, A. I., Paucar, N. E., Hibbert, M., Dudgeon, J. (2023). Integrating Microbial Fuel Cell and Hydroponic Technologies Using a Ceramic Membrane Separator to Develop an Energy-Water-Food Supply System. *Membranes*. *13(9)*, 803. [Crossref]

Sharma, S. C., Feng, C., Li, J., Hu, A., Wang, H., Qin, D., & Yu, C. P. (2016). Electrochemical Characterization of a Novel Exoelectrogenic Bacterium Strain SCS5, Isolated from a Mediator-Less Microbial Fuel Cell and Phylogenetically Related to Aeromonas jandaei. Microbes and environments, 31(3), 213-225. [Crossref]

Shirkosh, M., Hojjat, Y., Mahdi, M. M. (2022). Evaluation and optimization of the Zn-based microfluidic microbial fuel cells to power various electronic devices. *Biosensors and Bioelectronics: X*, *Vol. 12*,100254. [Crossref]

Sonaware, J.-M., Yadav, A., Ghosh, P.-C., Adeloju, S.-B. (2017). Recent advances in the development and utilization of modern anode materials for high performance microbial fuel cells. Biosensors and Bioelectronics: 90, 558-576. [Crossref]

Statistica, 2024. statista.com (accessed 26/02/2024)

Tamura, K., Stecher, G., & Kumar, S. (2021). MEGA11: molecular evolutionary genetics analysis version 11. Molecular biology and evolution, 38(7), 3022-3027. https://doi.org/10.1093/molbev/msab120

Tan, L., Li, S.-J., Wu, X.-T., Li, N., & Liu, Z.-Q. (2018). Porous Co3O4 decorated nitrogen-doped graphene electrocatalysts for efficient bioelectricity generation in MFCs. *International Journal of Hydrogen Energy*, *43*(22), 10311–10321. [Crossref]

Tian, P., Liu, D., Li, K., Yang, T., Wang, J., Liu, Y., & Zhang, S. (2017). Porous metal–organic framework $Cu_3(BTC)_2$ as catalyst used in air–cathode for high performance of microbial fuel

cell. *Bioresource technology*, *244*, 206–212. **[Crossref]**

Tou, Y., Azri, M., Sadi, M., Lounici, H. & kebbouche e-Gana, S. (2019). *Chlorophytum* microbial fuel cell characterization, *International Journal of Green Energy*, *16(12)*, 947-959. **[Crossref]**

Wang, C., Xing, Y., Zhang, K., Zheng, H., Zhang, Y., Zhu, X., Yuan, X., & Qu, J. (2023). Evaluation of photocathode coupling-mediated hydroxychloroquine degradation in a single-chamber microbial fuel cell based on electron transfer mechanism and power generation. *Journal of Power Sources*, *559*, 232625. **[Crossref]**

Wang, H., Li, J., Hu, A., Qin, D., Xu, H., Yu, C. P. (2013). *Melaminivora alkalimesophila* gen. nov., sp. nov., a melamine–degrading beta proteobacterium isolated from a melamine–producing factory. *Int J Syst Evol Microbiol*. *64*, 1938– 1944. **[Crossref]**

Web of Science, (2023). webofscience.com (accessed 10/01/2023)

Wolf, J., Johnston, R. B., Ambelu, A., Arnold, B. F., Bain, R., Brauer, M., Brown, J., Caruso, B. A., Clasen, T., Colford, J. M., Jr, Mills, J. E., Evans, B., Freeman, M. C., Gordon, B., Kang, G., Lanata, C. F., Medlicott, K. O., Prüss-Ustün, A., Troeger, C., Boisson, S., Cumming, O. (2023). Burden of disease attributable to unsafe drinking water, sanitation, and hygiene in domestic settings: a global analysis for selected adverse health outcomes. Lancet (London, England), 401(10393), 2060–2071. **[Crossref]**

Xing, D., Zuo, Y., Cheng, S., Regan, J. M., Logan, B. E. (2008). Electricity generation by *Rhodopseudomonas palustris* DX–1. *Environ Sci Technol42(11)*, 4146–4151. **[Crossref]**